

SALT Long-slit Spectroscopy of LBQS 2113+4538: variability of the Mg II and Fe II component^{*}.

K. Hryniewicz¹, B. Czerny¹, W. Pych¹, A. Udalski², M. Krupa³, A. Świątoń³, and J. Kaluzny¹

¹ Nicolaus Copernicus Astronomical Center, Bartycka 18, 00-716 Warsaw, Poland

² Warsaw University Observatory, Al. Ujazdowskie 4, 00-478 Warszawa, Poland

³ Astronomical Observatory of the Jagiellonian University, Orla 171, 30-244 Cracow, Poland

Received; accepted

ABSTRACT

Context. Mg II line is of extreme importance for intermediate quasars since it allows to measure the black hole mass in these sources and to use them as probes of the distribution of dark energy in the Universe, as a complementary tool to SN Ia.

Aims. Reliable use of Mg II requires good understanding of all systematic effects involved in the measurement of the line properties, including the contamination by Fe II UV emission.

Methods. We performed three spectroscopic observations of a quasar LBQS 2113-4538 with the SALT telescope separated in time by several months and we analyze in detail the mean spectrum and the variability in the spectral shape.

Results. We show that even in our good quality spectra the Mg II doublet is each well fit by a single Lorentzian shape, and the Fe II pseudo-continuum is well represented by one of the theoretical templates of Bruhweiler & Verner. The amplitudes of both components vary in time but the shapes do not change significantly. The measured line width of LBQS 2113+4538 puts this object into the class A quasars. The upper limit of 3% for the contribution of the NLR to Mg II may suggest that the separation the BLR and NLR disappears in this class of objects.

Key words. accretion, accretion disks – black hole physics

1. Introduction

Broad emission lines in Active Galactic Nuclei offer an insight into otherwise unresolved central parts. They probe the geometry, the inflow/outflow of the gas, and offer a way to measure the black hole mass relatively accurately. It was recently proposed that they can even be used to measure the expansion rate of the Universe since they obey a relation between the size of the emitting region and the absolute monochromatic luminosity (Watson et al. 2011, Czerny & Hryniewicz 2011). The most important emission lines are: H β for nearby sources, Mg II for intermediate redshift objects and CIV for high redshift quasars, Detailed studies of these lines are thus essential.

Extensive monitoring of over 50 nearby quasars and Seyfert galaxies showed that H β line intensity follows closely the variation of the continuum emission with very little scatter, and the line width is mostly determined by the Keplerian motion without significant inflow/outflow pattern (e.g. Peterson 1993, Kaspi et al. 2000, Peterson et al. 2004, Wandel et al. 1999, Bentz et al. 2013). This line now is thus broadly used for black hole mass determination. However, for sources at higher redshifts H β line moves out of the optical band to the IR and thus has to be replaced with another line.

In the intermediate redshift quasars Mg II 2800 Å line is an attractive option. Mg II line, as H β , belongs to the Low Ionization Line (LIL) class. These lines are thought to be emitted close to the accretion disk surface while High Ionization Lines (HIL), like CIV, come rather from outflowing wind and are strongly affected by varying conditions (Collin-Souffrin et

al. 1988). There were only a few examples of the Mg II monitoring in nearby objects (Clavel et al. 1991 for NGC 5548; Reichert et al. 1994 for NGC 3783; Peterson et al. 2004 for Fairall 9; Metzroth et al. 2006 for NGC 4151). The line was used instead of H β to determine the black hole mass from a single epoch spectra in quasar samples by Kong et al. (2006) and Vestergaard & Osmer (2009). Shen et al. (2008) analysis showed that Mg II is indeed a good proxy to H β line. On the other hand, Wang et al. (2009) at the basis of the study of SDSS intermediate quasars concluded that the velocity width of Mg II tends to be smaller than that of H β . In their fits, the authors were using the multiple component fit to Mg II and an Fe II pseudo-continuum template from Tsuzuki et al. (2006).

In this paper we present high quality medium resolution spectra of a quasar LBQS 2113-4538 ($z = 0.946 \pm 0.005$; Hewett et al. 1995) obtained with the RSS instrument of Southern African Large Telescope. The source was first identified in the objective-prism plates from the UK Schmidt Telescope (Morris et al. 1991) and included in the Large Bright Quasar Sample (Hewett et al. 1995) as well as in Veron-Cetty et al. (2001a) catalog. The previous studies indicated typical value of the Mg II line width and shape, and a simple line profile ($EW = 27^{+14}_{-11}$ Å, $FWHM = 4500 \pm 1100$ km s⁻¹ in Forster et al. 2001, and 4500 ± 550 km s⁻¹ in Vestergaard & Osmer 2009 for this source, and in the whole LBQS sample the median values are $EW = 33.8$ Å, $FWHM = 4440$ km s⁻¹ respectively, Forster et al. 2001). We analyze in detail the shape and the variability of the Mg II line as well as the underlying Fe II emission in this source.

^{*} based on observations made with the Southern African Large Telescope (SALT) under program 2012-1-POL-008 (PI: B. Czerny)

2. Observations

We performed three observations of the quasar LBQS 2113-4538 using the Robert Stobie Spectrograph (RSS; Burgh et al. 2003, Kobulnicky et al. 2003; Smith et al. 2006) on Southern African Large Telescope (SALT) in the service mode. The data was collected in three blocks, in the nights May 15/16, July 30/31, and November 18/19, 2012 (UT) thus covering the period of 6 months. Each block consisted of a pair of 978 second exposures of the target spectrum in a long slit mode, with the slit width of 2", followed by an exposure of the spectrum of the Argon calibration lamp, and a set of flat-field images. We used RSS PG1300 grating, with the spectral resolution of $R = 1047$ at 5500 Å, and the PC04600 filter. The observations were performed in a Dark Moon, Bright Moon and Grey Moon conditions. The nights were not photometric, in particular the third (Grey Moon) observation has been performed in the presence of thin clouds. Initial data reduction steps: gain correction, cross-talk correction, overscan bias subtraction and amplifier mosaicking have been performed by the SALT Observatory staff using a semi-automated pipeline from the SALT PyRAF package¹ (see Crawford et al. 2010). Flat-field correction and further reduction steps have been performed using procedures within the IRAF package. The pairs of adjacent spectrum images of LBQS 2113-4538 have been combined into a single image. This enabled us to efficiently reject cosmic rays and raise the signal to noise ratio. Identification of the lines in the calibration lamp spectrum, wavelength calibration, image rectification and extraction of one dimensional spectra have been done using functions from `nao.twospec` package within IRAF².

The spectroscopic observations were supplemented with the seven photometric observations in V band by the OGLE team. The source was weakly but significantly variable, as measured with respect to the three comparison stars.

Here we analyze in detail the limited spectral band between 2700 and 2900 Å rest frame with the aim to reproduce the behavior of the Mg II and Fe II emission.

To perform flux calibrations we used the star TYC 8422-788-1 from Hipparcos catalog located in the slit and separated by 3.5 arc min from the quasar. The star, according to the Piquard et al. (2001) is a variable star³ of δ Cephei type, with a V band luminosity 11 mag and a period of 8.740332 days. Such stars have typically the temperature varying between 5000 K and 6000 K, and surface gravity of order of 1.5 - 2.3. We extracted the spectra of the star with the same procedure as for the quasar. Next we used the Castelli & Kurucz (2004) model assuming the effective temperature 5500 K, surface gravity 1.5 and solar metallicity. We divided the observed spectrum of the star by the atmosphere model. The ratio was fitted with the third order polynomial thus creating the response function. The wavelength range above 5000 K was in the Wien tail and the models gave the same spectral shape, independently from assumptions for the star temperature and gravity.

This response function was then applied to each of the quasar spectra in the 5100 - 5700 Å range in the observed frame. In the

actual data fitting, only the narrower region (2700 - 2900 Å in the rest frame) was used.

We estimated the instrumental broadening close to the Mg II using the 5200 Å sky line to be 135 ± 7 km s⁻¹ for the lowest quality Observation 3. This value is much narrower than the expected line width so in the data fitting we neglect this effect. We actually checked in one example that introducing the instrumental broadening leads to marginally narrower lines by ~ 100 km s⁻¹.

Finally, the spectra were deredened to account for the Galactic extinction assuming $A_V = 0.150, 0.113$ and 0.090 in B, V and R band for this source (Schlafly & Finkbeiner 2011) after NED⁴ with quadratic extrapolation between these values for other wavelengths.

Next, we obtained the mean spectrum by adding the three spectra together. We then analyzed both the mean spectrum as well as the individual spectra in search of the variability in the spectral shape.

We neglect the intrinsic absorption as there is no clear signature of such extinction in the spectra. We also neglect possible host galaxy contribution as it is not likely to be important at such short wavelengths.

3. Model

We modeled the spectrum assuming the following components: power law continuum, Fe II pseudo-continuum and Mg II modeled either as a single line at 2800 Å or as a doublet (2796.35, 2803.53; Morton 1991). The doublet ratio was found to be 1,2:1 in I Zw 1 FOS/HST data implying the optically thick case, and in our considerations we fixed this ratio at 1:1. The redshift of the object is treated as an arbitrary parameter since the determination by Forster et al. (2001) is not accurate from the point of view of our high quality spectroscopy. The 2700 - 2900 Å region is also contaminated by the Balmer continuum (see e.g. Dietrich et al. 2001) but this component is shallow in the limited wavelength region so this component cannot be distinguished from the underlying power law. This effect slightly influences the fitted power law slope but not the normalization of the Fe II component or the Mg II shape.

Single Mg II component is modeled either as a Gaussian, or Lorentzian. We also tried two-component Gaussian fit, as well as rotationally broadened Lorentzian, following Kollatschny & Zetzl (2013).

The Fe II UV emission is modeled with the use of several templates, both theoretical and observational. We start with the Vestergaard & Wilkes (2001) template, based on I Zw 1 with zero contribution underlying MgII core, and the template of Tsuzuki et al. (2006) also based on I Zw 1 but with some Fe II emission underlying Mg II obtained by subtraction of the two Gaussian modeling the Mg II doublet. Next we experiment with purely theoretical templates of Bruhweiler and Verner (2008), obtained by varying the density, turbulent velocity and ionization parameter Φ . We allow for Fe II broadening as well as for the shift with respect to Mg II since Fe II was suggested to come from infalling material (Ferland et al. 2009).

4. Results

We model the three high quality RSS SALT spectra of LBQS 2113+4538 in the 2700 Å - 2900 Å rest frame as consisting of

¹ <http://pysalt.salt.ac.za>

² IRAF is distributed by the National Optical Astronomy Observatories, which are operated by the Association of Universities for Research in Astronomy, Inc., under cooperative agreement with the NSF.

³ <http://cdsarc.u-strasbg.fr/cgi-bin/nph-Cat/html/max=107?II/233/tableb-v.dat>

⁴ NASA/IPAC Extragalactic Database (NED) is operated by the Jet Propulsion Laboratory, California Institute of Technology

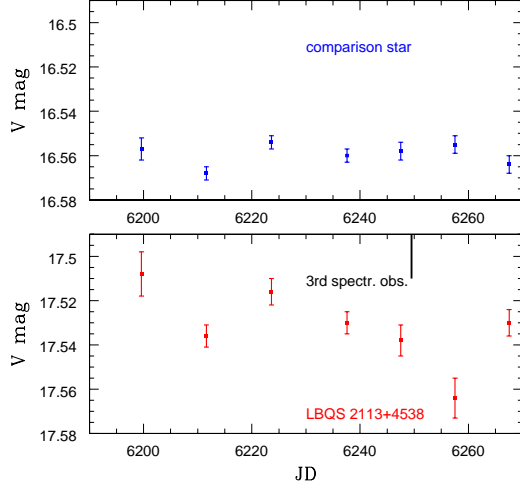


Fig. 1. The V band lightcurve of LBQS 2113+4538 (lower panel) and one of the comparison stars (upper panel); the last spectroscopic observation was performed during this photometric campaign.

the power law continuum, Fe II pseudo-continuum and Mg II line. The observation span covers 6 months. The photometric observations, covering similar period, show clear although not very strong variations, with the amplitude of ~ 0.03 mag. The lightcurve and one of the three comparison stars are shown in Fig. 1.

4.1. Mean spectrum

Since the variability is not very strong, we started with the composite of the three spectra. The fits are summarized in Table 1. Line and pseudo-continuum EW was calculated in the 2700 - 2900 Å band where the fit was performed, and both were calculated with respect to the power law continuum. The statistical errors for the best fit parameters are typically of order of 0.3 Å for EW(Mg II) and 2.0 Å for EW(Fe II), 50 - 100 km s⁻¹ for Mg II kinematic width. The Fe II smearing velocity was mostly fixed but we tested a few possible values, and the implied accuracy of the values given in the table is about 100 - 200 km s⁻¹.

The frequently used Fe II pseudo-continuum template of Vestergard & Wilkes (2001), combined with Gaussian or Lorentzian shape of the Mg II line did not provide the satisfactory fit to the data. In Fig. 2 we show the best fit for a Lorentzian shape, doublet with the equal intensity of the components (model C), together with residuals. Strong residuals are clearly seen. The use of the templates from Tsuzuki et al. (2006) only partially reduces the residuals.

However, we obtained very interesting results for the theoretical templates of Fe II from Bruhweiler and Verner (2008), which were recently applied to a large sample of SDSS quasars (Marziani et al. 2013). These templates give systematic residuals at 2950 Å due to the absence of Fe I emission in the model (see Marziani et al. for the discussion) but our fits did not extend so far. The best fit for the model E was fully satisfactory, no significant patterns are seen (see Fig 3), and the χ^2/dof dropped

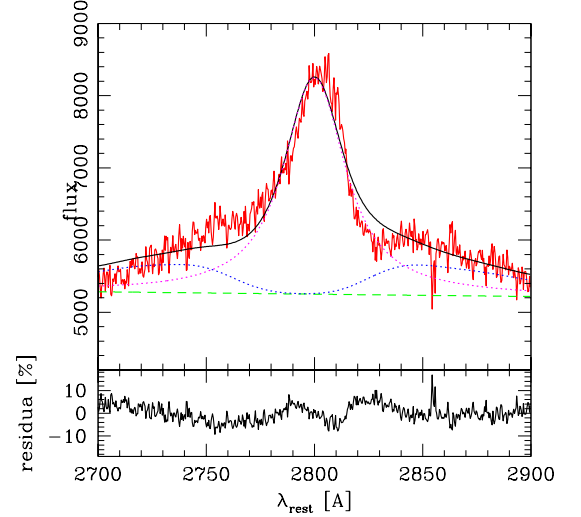


Fig. 2. The best fit and fit components (upper panel: total model - continuous line, continuum - green dashed line, continuum with Fe II pseudo-continuum - blue dotted line, Mg II component with continuum - red dotted line and residuals (lower panel) for the mean spectrum (red continuous line) for model C (see Table 1 for the model parameters).

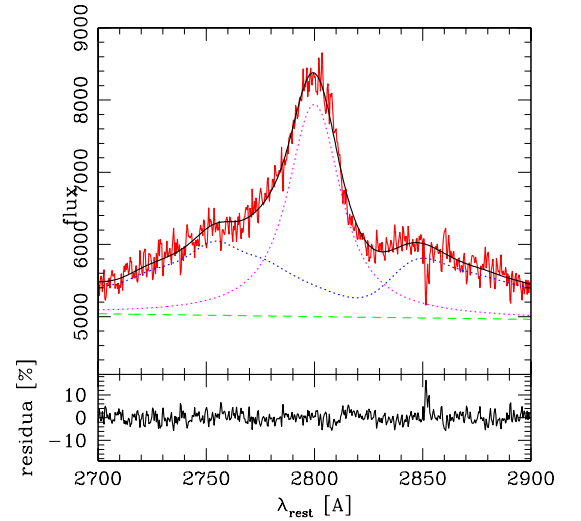


Fig. 3. The best fit and residuals for the mean spectrum, as in Fig. 2 but for model E.

almost by a factor of three!. It was frequently argued that the Lorentzian shape provides a very good description and our high quality spectra support this conclusion. All the complexities of the nearby wavelength range are satisfactorily explained by complexity of the Fe II component. In particular, the strong pattern at ~ 2750 Å and somewhat weaker feature at ~ 2850 Å in the total spectrum are then nicely reproduced. The exact pa-

rameters of the best theoretical template (model E) are: model with 735 atomic levels, number density $n_H = 10^{11} \text{ cm}^{-3}$, turbulent velocity $v_{turb} = 20 \text{ km s}^{-1}$ and $\Phi = 10^{20.5} \text{ cm}^{-2} \text{ s}^{-1}$. Interestingly, Bruhweiler and Verner (2008) came to the same conclusion when analysing the I Zw I spectrum.

Several other theoretical templates from Bruhweiler and Verner (2008) gave worse, but still reasonable fits (models F and L). The worst fit was for the model J and K which suggests that $v_{turb} > 10 \text{ km s}^{-1}$. The comparison of model L and P strongly favors densities lower than 10^{12} cm^{-3} .

We tested whether allowing for a velocity shift of the Fe II pseudo-continuum and Mg II line improves the fit. However, we have not found any evidence for such a difference, with the upper limit for the relative velocity of 300 km s^{-1} .

We also checked whether the rotationally broadened Lorentzian shape, justified theoretically (see e.g. Kollatschny & Zetzl 2013) provides a better fit than a single Lorentzian. However, when we considered the intrinsic width of the Lorentzian much narrower than the rotational broadening, the fit quality dropped. Better fits than for a single Lorentzian were obtained when the rotational broadening was smaller than the intrinsic width, but the change was not actually significant (the drop in χ^2 below 2.0). It does not mean that there is no rotational component in the line; it only shows that this rotational broadening is not well reproduced by the orbital motion of the spherically distributed clouds.

4.2. Separate spectra

We next analyse the three spectra separately because the observational conditions were significantly different in all three observations, and the source did vary, as shown by the photometric measurements.

First (the earliest) spectrum is of the highest quality, obtained in the dark moon condition, with the sky background by a factor of almost 3 lower than the continuum flux.

We used the same models, as before. Again, the Fe II template of Vestergaard & Wilkes (2001) gave poor fit and clearly visible residuals (see Fig. 4) while the use of theoretical templates reduced all residuals very strongly. The best fit was obtained for model E, as in the case of the mean spectrum. In Fig. 5 we show the best fit and the residuals, with statistical errors giving $\chi^2/dof = 684.5/562$. Systematic errors are too difficult to estimate, particularly in the case of such a complex instrument as SALT. However, the residuals do not show considerable pattern. Large deviations at 2850 \AA (rest frame) are due to imperfect subtraction of the sky line. Not much worse fits are again obtained for models F and L, and the worst fits again for models J and K. Better fit for other templates can be obtained assuming at least two separate components for the Mg II. For example, in Fig. 6 we show such a two-component Mg II fit combined with Tzuzuki et al. (2006) templates. The fit quality is only slightly worse than for a single-component model E (χ^2 of 712.9 vs. 684.4). The two Mg II components have the FWHM of 1600 and 2890 km s^{-1} , correspondingly, and they are blueshifted in velocity space by 1390 km s^{-1} . Both components are then comparably broad, so the satisfactory interpretation of such a fit is rather difficult, since none of the components correspond to the contribution from the Narrow Line Region (NLR). The statistical errors for the best fit parameters in these data set are typically of order of 0.1 \AA for EW(Mg II), better than for the mean spectrum.

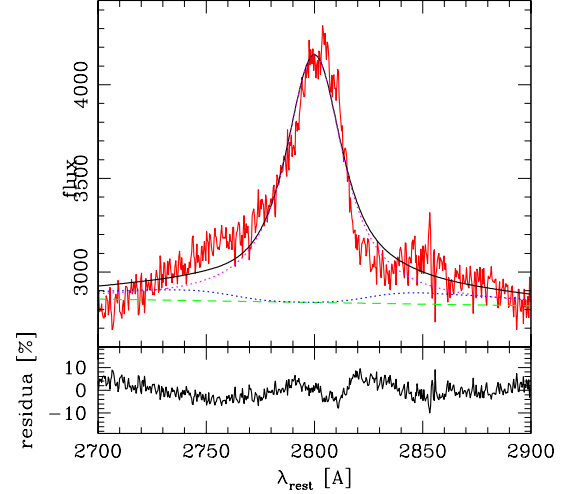


Fig. 4. The best fit and residuals for the Observation 1, model C (see Table 2 for model parameters and Fig. 2 for the description of individual curves).

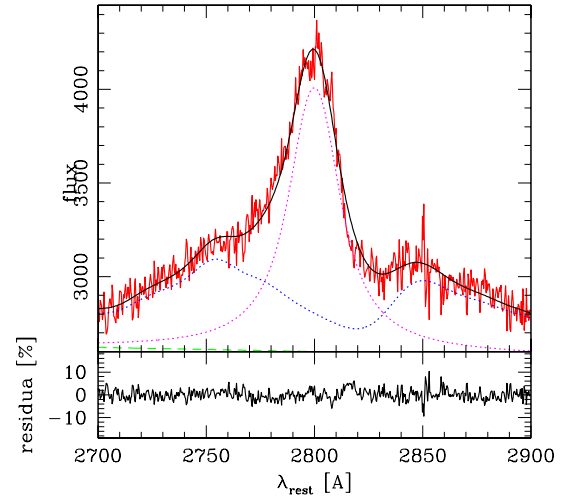
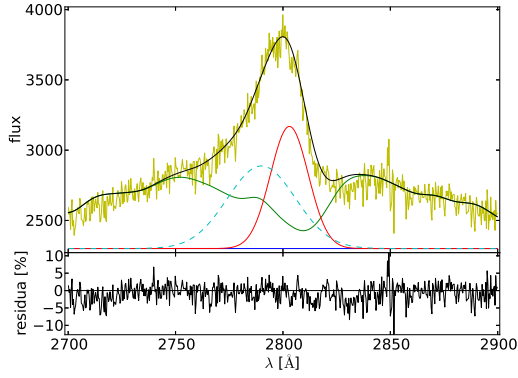
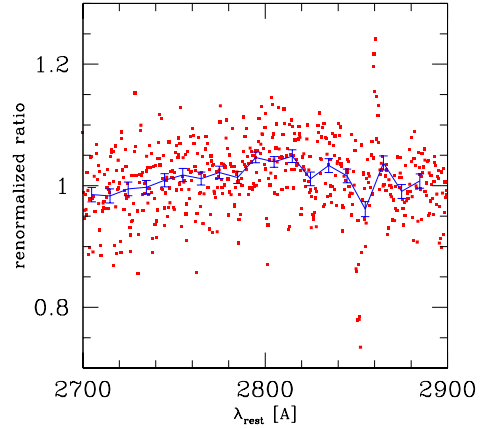


Fig. 5. The best fit and residuals for the Observation 1, model E (see Table 2 for model parameters and Fig. 2 for the description of individual curves).

The second spectrum, obtained in the Bright Moon conditions, has much higher sky background flux, dominating the source by a factor of 8. Statistical errors are then the dominant source of the error, and satisfactory fits can be obtained. The Fe II template of Vestergaard & Wilkes (2001) did not represent the data well, but theoretical models gave again interesting results. The best fit was for model F, i.e. for the case of the somewhat higher turbulent velocity ($v_{turb} \sim 30 \text{ km s}^{-1}$ instead of 20) than in the first observation. However, the χ^2 for model E was only by 4.1 lower, so within two sigma error. The worst solutions were

Table 1. Parameters of the fits for the mean spectrum.

Model	S/D	Line shape	Fe II template	Fe II Width km s ⁻¹	slope	z	Mg II EW Å	Mg II FWHM km s ⁻¹	Fe II EW Å	χ^2
A	Single	Gauss	Vestergaard	1200	-0.13	0.954	14.64	3530	1.47	1680.9
B	Single	Lorenzian	Vestergaard	1200	-0.15	0.954	20.69	3200	0.18	1230.0
C	Doublet	Lorenzian	Vestergaard	1200	-0.14	0.954	20.80	3140	0.27	1238.5
D	Single	Lorenzian	d11-m20-20.5-735	900	-0.22	0.956	24.78	3050	25.62	520.2
E	Doublet	Lorenzian	d11-m20-20.5-735	900	-0.22	0.956	23.81	2800	24.77	507.3
F	Doublet	Lorenzian	d11-m30-20.5-735	1100	-0.20	0.956	23.61	2800	23.89	530.0
G	Doublet	Lorenzian	Tsuzuki	900	-0.30	0.956	22.85	2600	23.46	891.9
H	Doublet	Lorenzian	d11-m20-21-735	1100	-0.23	0.956	23.53	2750	25.04	537.2
I	Doublet	Lorenzian	d10-5-m20-20-5	1100	-0.02	0.956	23.02	2800	23.11	582.5
J	Doublet	Lorenzian	d11-m05-20-5	1100	0.00	0.956	22.34	2800	18.86	608.4
K	Doublet	Lorenzian	d11-m10-20-5	1100	0.13	0.956	22.85	2800	21.87	594.4
L	Doublet	Lorenzian	d11-m20-20-5	1100	0.25	0.956	23.52	2800	26.33	533.1
M	Doublet	Lorenzian	d11-m30-20-5	1100	0.32	0.956	24.56	2900	28.34	552.7
N	Doublet	Lorenzian	d11-m50-20-5	1100	0.47	0.956	25.52	2900	32.88	541.4
O	Doublet	Lorenzian	d11-5-m20-20-5	1100	0.20	0.956	23.97	2850	24.07	570.6
P	Doublet	Lorenzian	d12-m20-20-5	1100	0.24	0.956	23.89	2800	22.11	567.6
Q	Doublet	Lorenzian	d11-m20-20	1100	0.23	0.956	23.67	2800	24.29	560.3
R	Doublet	Lorenzian	d11-m20-21	1300	0.31	0.956	23.93	2800	29.77	559.4

**Fig. 6.** The best fit and the residua for Tsuzuki et al. Fe II template and two Gaussian model for Mg II LBQS 2113+4538.**Fig. 7.** The normalized ratio of the data points from Observation 2 to Observation 1 (red points - original data, blue line with errorbars - data binned in wavelength by a factor of 30).

again for models J and K. The line kinematic width measured by various models in observation 2 was slightly higher than in the observation 1, but the change was within 2 sigma error. The EW of the line clearly increased, in most models rising by $\sim 25\%$, and the EW of the Fe II component also increased. Detailed assesment of the change in these two components is postponed to Sect. 4.4. The statistical errors for the best fit parameters in Observation 2 are typically of order of 0.3 Å for EW(Mg II), comparable to the results for the mean spectrum.

The third spectrum was obtained in the most difficult conditions, with the Grey Moon but with some intervening clouds. The background did not dominate the source so much as in the previous case, only by a factor of 3. Statistical errors are very large, the EW(Mg II) is determined with a large error (for example, for model E, we have $23.79^{+2.26}_{-2.07} \text{ Å}$). Also systematic errors are large since the signal directly measured by the telescope was by a factor of 3 lower due to the cloud extinction. However, the model E again was the best, and model N the worst one, among the models based on theoretical templates. The line was relatively weaker during this observation, and the spectrum was much steeper.

None of the spectra show any narrow intrinsic absorption features.

4.3. Non-parametric variability test

We tested the variations of the spectral shape of the quasar simply by dividing the second spectrum by the first one. The renormalized ratio, with the average value set to 1, shows considerable curvature due to the variations in Mg II and Fe II strongly dominating the spectrum in its middle part (see Fig. 7). The linear fit to the ratio indicates also the overall change of the continuum slope, as seen in the model fits, which is quantitatively consistent with the change of the power law slope by 0.2 between the two data sets.

Table 2. Parameters of the fits for the three individual spectra obtained with SALT between May and November 2012.

Model	S/D	Line shape	Fe II template	Fe smear	slope	z	Mg II EW Å	Mg II FWHM km s ⁻¹	EW Fe II EW Å	χ^2
Obs. 1										
A	Single	Gauss	Vestergaard	1200	-0.11	0.954	14.23	3530	2.86	2167.4
B	Single	Lorentzian	Vestergaard	1200	-0.18	0.954	20.83	3350	2.32	1556.1
C	Doublet	Lorentzian	Vestergaard	1200	-0.18	0.954	20.54	3150	2.60	1569.9
D	Single	Lorentzian	d11-m20-20.5-735	900	-0.24	0.956	21.78	2950	22.04	707.8
E	Doublet	Lorentzian	d11-m20-20.5-735	900	-0.24	0.956	21.33	2690	22.48	684.4
F	Doublet	Lorentzian	d11-m30-20.5-735	1100	-0.16	0.956	22.43	2750	26.88	712.9
G	Doublet	Lorentzian	Tsuzuki	900	-0.26	0.956	21.69	2500	26.74	1274.2
H	Doublet	Lorentzian	d11-m20-21-735	1100	-0.23	0.956	21.46	2680	23.66	741.2
I	Doublet	Lorentzian	d10-5-m20-20-5	1100	0.28	0.956	22.31	2800	26.09	778.9
J	Doublet	Lorentzian	d11-m05-20-5	1100	0.06	0.956	19.36	2650	15.39	863.4
K	Doublet	Lorentzian	d11-m10-20-5	1100	0.18	0.956	21.29	2750	22.20	832.1
L	Doublet	Lorentzian	d11-m20-20-5	1100	0.25	0.956	21.71	2750	26.70	728.5
M	Doublet	Lorentzian	d11-m30-20-5	1100	0.25	0.956	22.15	2800	26.28	758.1
N	Doublet	Lorentzian	d11-m50-20-5	1100	0.40	0.956	23.33	2900	30.22	741.4
O	Doublet	Lorentzian	d11-5-m20-20-5	1100	0.16	0.956	21.79	2800	21.94	786.7
P	Doublet	Lorentzian	d12-m20-20-5	1100	0.22	0.956	22.36	2800	21.70	778.1
Q	Doublet	Lorentzian	d11-m20-20	1100	0.20	0.956	21.70	2750	23.28	756.3
R	Doublet	Lorentzian	d11-m20-21	1300	0.30	0.956	21.72	2700	28.72	778.2
Obs. 2										
A	Single	Gauss	Vestergaard	1200	0.08	0.954	20.26	3940	9.55	777.5
B	Single	Lorentzian	Vestergaard	1200	0.08	0.954	29.20	3750	7.61	649.5
C	Doublet	Lorentzian	Vestergaard	1200	0.08	0.954	28.65	3500	8.11	653.8
D	Single	Lorentzian	d11-m20-20.5-735	900	-0.05	0.956	25.22	3050	21.03	484.2
E	Doublet	Lorentzian	d11-m20-20.5-735	900	0.00	0.956	26.54	2870	26.65	476.3
F	Doublet	Lorentzian	d11-m30-20.5-735	1100	0.05	0.956	26.05	2850	26.42	478.2
G	Doublet	Lorentzian	Tsuzuki	900	0.03	0.956	28.16	2650	38.21	550.6
H	Doublet	Lorentzian	d11-m20-21-735	1100	0.00	0.956	26.05	2850	26.34	478.8
I	Doublet	Lorentzian	d10-5-m20-20-5	1100	0.50	0.956	26.01	2900	26.42	484.1
J	Doublet	Lorentzian	d11-m05-20-5	1100	0.30	0.956	23.10	2750	17.05	497.2
K	Doublet	Lorentzian	d11-m10-20-5	1100	0.44	0.956	25.29	2900	24.17	489.3
L	Doublet	Lorentzian	d11-m20-20-5	1100	0.61	0.956	27.15	2900	31.92	478.7
M	Doublet	Lorentzian	d11-m30-20-5	1100	0.61	0.956	27.72	3000	31.36	481.8
N	Doublet	Lorentzian	d11-m50-20-5	1100	0.83	0.956	29.16	3050	37.15	480.5
O	Doublet	Lorentzian	d11-5-m20-20-5	1100	0.38	0.956	25.88	2900	23.36	480.5
P	Doublet	Lorentzian	d12-m20-20-5	1100	0.46	0.956	26.34	2900	22.78	485.1
Q	Doublet	Lorentzian	d11-m20-20	1100	0.48	0.956	26.42	2920	25.99	484.7
R	Doublet	Lorentzian	d11-m20-21	1300	0.61	0.956	27.08	2900	33.48	480.9
Obs. 3										
A	Single	Gauss	Vestergaard	1200	-1.03	0.954	20.91	3825	14.00	373.0
B	Single	Lorentzian	Vestergaard	1200	-1.11	0.954	31.74	3700	14.20	323.1
C	Doublet	Lorentzian	Vestergaard	1200	-1.10	0.954	31.84	3600	14.05	325.0
D	Single	Lorentzian	d11-m20-20.5-735	900	-1.12	0.956	24.69	2950	21.49	237.7
E	Doublet	Lorentzian	d11-m20-20.5-735	900	-1.09	0.956	23.79	2650	22.43	237.3
F	Doublet	Lorentzian	d11-m30-20.5-735	1100	-1.09	0.956	24.22	2720	21.99	240.3
G	Doublet	Lorentzian	Tsuzuki	900	-1.13	0.956	24.550	2450	29.054	262.8
H	Doublet	Lorentzian	d11-m20-21-735	1100	-1.07	0.956	28.48	2700	42.39	292.0
I	Doublet	Lorentzian	d10-5-m20-20-5	1100	-0.68	0.956	23.52	2650	22.74	242.9
J	Doublet	Lorentzian	d11-m05-20-5	1100	-0.80	0.956	21.63	2625	13.78	247.2
K	Doublet	Lorentzian	d11-m10-20-5	1100	-0.70	0.956	23.52	2650	22.40	248.7
L	Doublet	Lorentzian	d11-m20-20-5	1100	-0.45	0.956	24.74	2600	33.85	250.3
M	Doublet	Lorentzian	d11-m30-20-5	1100	-0.53	0.956	26.79	2900	31.53	248.5
N	Doublet	Lorentzian	d11-m50-20-5	1100	0.35	0.956	36.12	3100	66.83	312.6
O	Doublet	Lorentzian	d11-5-m20-20-5	1100	-0.35	0.956	30.50	3000	40.41	295.9
P	Doublet	Lorentzian	d12-m20-20-5	1100	-0.45	0.956	27.33	2800	30.23	266.1
Q	Doublet	Lorentzian	d11-m20-20	1100	-0.70	0.956	24.30	2775	21.83	243.8
R	Doublet	Lorentzian	d11-m20-21	1300	-0.70	0.956	23.48	2700	23.03	243.2

4.4. Variations of EW of Mg II and Fe II and relative shifts

We found that the photometric variations in the source are accompanied by the spectral variability. Selecting model E for a comparison of the three spectra, we observed an increase of the

EW(Mg II) by 24.4 % between the second and the first observation, followed by a decline in the third one. EW(Fe II) varied in a similar way. The ratio of EW(Mg II)/EW(Fe II) was constant within the measurement error, but the accuracy if the

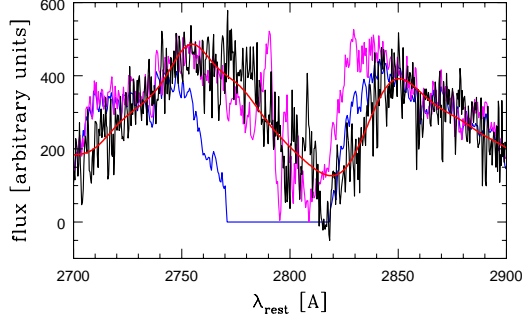


Fig. 8. The comparison of various templates used to model Fe II pseudo-continuum in UV band: Vestergaard & Wilkes (2001) - blue line, Tsuzuki et al. (2006) - magenta line, our newly proposed template - black line, 11-m20-20.5-735 of Bruhweiler & Verner (2008) convolved with 900 km/s Gaussian broadening, as used in the current paper - red thick line.

Fe II measurement is not very high (the ratio of EW(Fe II) in the Observation 2 to Observation 1 is 1.19 ± 0.1). The errors in Observation 3 are still larger, so we cannot treat the conclusion about the common temporal variability of Mg II and Fe II with high confidence. The kinematic width of the Mg II line did not show any significant variations, with an upper limit of 14 %. Similar lack of the Mg II line (broad component) shape variability despite the variations of the line intensity was observed for NGC 3516 (Goad et al. 1999). Woo (2008) in the two-year campaign observed the change in the line kinematic width by 8 to 17 %. The Mg II line is broader than the requested broadening of the Fe II template (1350 km s^{-1} vs. 900 km s^{-1}) so Fe II may come from a somewhat larger distance. The slope of the underlying continuum also changed, but in uncorrelated pattern with EW(Mg II).

We also looked for solutions allowing for an arbitrary kinematic shifts between the position of Mg II and Fe II which would be interpreted as a signature of inflow or outflow for one of the components. In Observation 1, the best fit was actually obtained for a relative velocity of $45^{+24}_{-33} \text{ km s}^{-1}$ (two sigma error), indicating marginal hints of Mg II inflow if Fe II is in rest, or Fe II outflow if Mg II provides the reference. In the other two observations the data quality is too low to see any significant shift between Mg II and Fe II.

4.5. Fe II observational template

The issue of the Fe II contribution to the optical and UV spectrum has been recognized long time ago (Netzer & Wills 1983; Collin-Souffrin & Dumont 1986). There has been noticeable effort to treat this, but the issue is still not finally set.

We use the Observation 1 data to determine a new Fe II template in the 2700 - 2900 Å range by subtracting the fitted

powerlaw and the Mg II doublet from the total spectrum. The comparison of such a template with the previously used observational template and with the theoretical template 11-m20-20.5-735 of Bruhweiler & Verner (2008), broadened with a 900 km s^{-1} Gaussian are shown in Fig. 8. Such a template can be applied to sources with the intrinsic broadening greater than $\sim 900 \text{ km s}^{-1}$. We removed four observational points close to 2850 Å since in this region the extraction of the very strong sky line was not perfect, but this does not change the overall shape, densely covered.

The main difference between the newly proposed template and the Tsuzuki et al. (2006) template is in the 2820 - 2840 Å range. This would affect the modelling of the blue wing of the Mg II line. Otherwise, their template, obtained for a nearby object (I Zw 1) has somewhat better S/N ratio.

4.6. Global parameters

Determination of the Mg II line width opens a possibility to estimate the global parameters of the LBQS 2113+4538. We can estimate the black hole mass and the Eddington ratio is this object using various formulae applicable to the UV spectral range. The SALT spectroscopic observation does not provide an absolute calibration. We thus adopt V mag of 17.29 from Hewett et al. (1995) and correct it for the Galactic extinction $A_V = 0.113$ from NED. Using the standard cosmology, $H_0 = 71 \text{ km s}^{-1} \text{ Mpc}^{-1}$, $\Omega_m = 0.270$, $\Omega_\Lambda = 0.730$ we obtain the monochromatic luminosity of $1.24 \times 10^{46} \text{ erg s}^{-1}$ at 2800 Å. We then apply the formulae based on the 3000 Å continuum and Mg II line measurements. The bolometric luminosity is $7.32 \times 10^{46} \text{ erg s}^{-1}$ for a bolometric correction factor of 5.9 (McLure & Dunlop 2004). FWHM of the Mg II line for our model E fits in observation 1 is 2690 km s^{-1} (i.e. twice larger than the values quoted in Table 2). Using the formulae of Kollmeier et al. (2006), McGill et al. (2007), or Trakhtenbrot & Netzer (2012), we obtain the values of the black hole mass of $1.03 \times 10^9 M_\odot$, $4.72 \times 10^8 M_\odot$, $8.05 \times 10^8 M_\odot$ and the Eddington ratios of 0.57, 1.23, and 0.72, correspondingly. This ratio is somewhat higher than the value of 0.42 derived by Vestergaard & Osmer (2009), mostly due to much narrower line kinematic width in our fits.

5. Discussion

We analyzed three long-slit spectroscopic observations of the quasar LBQS 2113+4538, with the aim to analyse the shape and the variability of the Mg II broad emission line and Fe II pseudo-continuum.

The object shows clear variations in all spectral components. The Mg II line is measured very accurately in the first two observations, with an EW error of 0.1 Å and 0.3 Å, respectively, in the third one is of lower quality due to the clouds. The line varied by 25 % during the six month period. This shows that reverberation study of distant quasars can be done with the SALT telescope. The level of the Fe II pseudo-continuum is measured much less accurately since it is strongly coupled to the varying slope and normalization of underlying continuum. The ratio of the Fe II and Mg II did not change significantly but longer observations would be needed to give a firm statement at this issue. The kinematic broadening is slightly higher for Mg II than for Fe II (FWHM of 2700 and 1800 km s^{-1} , respectively) that would rather suggest Fe II origin at somewhat larger distances.

The shape of the Fe II pseudo-continuum is best modeled by one of the theoretical templates of Bruhweiler & Verner (2008).

The same template was found to be best for I Zw I by these authors. This, and the Lorentzian shape of Mg II indicate a considerable similarity between LBQS 2113+4538 and I Zw I, apart from much broader line kinematic width in the first case. It supports the deep meaning in the division of the quasars into A and B class sources, as proposed by Sulentic et al. (2007).

5.1. Nature of the BLR in type A quasars

The Mg II line, despite very high quality of the data, is well modeled with a single Lorentzian shape. We took into account the doublet character of the line (this improved the χ^2 by 23.4, although the doublet is not visibly resolved due to the broadening). The quasar is thus similar to NLS1 I Zw I, but the Mg II line is broader, with FWHM of 2690 km s⁻¹. Therefore the source does not belong to NLS1 as defined by Osterbrook & Pogge (1985), but it is a very good representative of the class A quasars, as defined by Sulentic et al. (2007), which likely forms the same source class but for objects with much higher black hole mass.

This class of the sources is characterized by relatively narrow permitted lines (below 2000 km s⁻¹ for NLS1, below 4000 km s⁻¹ for type A quasars), the permitted lines have Lorentzian profiles, strong Fe II emission, relatively small optical variability, but with occasional flares, relatively large X-ray variability, and their X-ray spectra are dominated by strong soft X-ray excess, followed by a steep hard X-ray power law (Boller, Brandt & Fink 1996; Brandt, Mathur & Elvis 1997; Leighly 1999; Wang & Netzer 2003; Gallo 2006; Panessa et al. 2011; Marziani et al. 2013; Ai et al. 2013). These properties are likely connected with the accretion at the levels close to Eddington ratio (e.g. Pounds et al. 1995; Mineshige et al. 2000; Grupe 2004; Collin et al. 2006). NLS1 galaxies have bolometric luminosities similar to BLS1 galaxies, but masses of order of 10⁷ M_⊙ (Wandel, Peterson & Malkan 1999; Grupe & Mathur 2004; Whalen et al. 2006), while the class A quasars have again luminosities typical for quasars, but masses at the lower end of quasar black hole masses. The object studied in this paper has also the black hole mass in the range 0.5 – 1 billion solar masses, and Eddington ratio in the range 0.6 – 1.2, depending on the adopted formulae. We do not have any constraints on the X-ray properties of this source.

The detailed analysis of the H β profiles for NLS1 galaxies and type A quasars strongly suggests a single component, if Lorentzian instead of Gaussians are used (e.g. Veron-Cetty et al. 2001b, Sulentic et al. 2002, Zamfir et al. 2010). In FOS/HST I Zw I spectrum of Mg II (which belongs to Low Ionization Lines, as H β), the Mg II doublet is actually resolved, but there seems to be no need for two separate NLR and BLR component (Laor et al. 1997). The same conclusion was reached by Shapovalova et al. (2012) who analyzed H β profile in 11-years observational campaign of the NLS1 galaxy Ark 564: the rms and mean profile for H β are identical (but other lines are not). However, as Shapovalova et al. (2012) stress, the decomposition of H β into putative NLR and BLR component is difficult due to the narrowness of the second one.

In LBQS 2113+4538 the Mg II line is broader, so the contribution from the NLR should be easily visible in our high quality data, but when fitting the line profiles we did not see immediate need for an additional narrow feature. We therefore made tests, by fixing the FWHM of the NLR component at 600 km s⁻¹ and allowed the normalization to vary. In the case of Observation1 we obtained the upper limit of 3 % at two sigma level of such a narrow component in Mg II. This upper limit is not consistent

with usual expectations of the $\sim 20\%$ contribution of the NLR to permitted lines (Contini et al. 2003, Shapovalova et al. 2012).

It thus seems that in NLS1/Type A quasars not only the BLR moves outward from the black hole in high Eddington ratio sources, but likely the NLR moves inward (it does not disappear, since the forbidden lines, like [O III] 5007 Å is usually intense in NLS1 objects, and the usual gap between BLR and NLR in permitted lines disappears. This gap exists due to the presence of dust, as argued by Netzer & Laor (1993). It is possible, that the significant change in the broad band continuum shape when passing from BLS1/Type B sources to NLS1/Type sources affects the computations presented in that paper.

While a single component fit for the permitted lines is very interesting, its Lorentzian shape may seem puzzling. Such a shape is natural in the case of atomic processes, but in AGN the line shape is determined by the combination of the density and velocity field. Lorentzian - instead of Gaussian - profile, with its broad, extended wings suggests an extended complex emitter, which leads the λ^{-2} shallow decay in the wings due to the combination of the two factors.

5.2. Selection of objects for cosmological application

The understanding of the formation of BLR in AGN, and in particular of the properties of Mg II line is important in a much broader context. As proposed by Watson et al. (2011), BLR size scaling with absolute luminosity offers a possibility to use AGN as probes of the expansion rate of the Universe. The scaling for H β is well studied observationally (see Bentz et al. 2013 for the most recent studies), and the same scaling is expected for Mg II at the basis of the theoretical understanding of the scaling mechanism (Czerny & Hryniewicz 2011). This line can be used for optical monitoring of medium redshift quasars but the attention should be paid to the proper selection of the sources based on the line shape in order to avoid unwanted line variability unrelated to the changes in the continuum (see Czerny et al. 2013). LBQS 2113+4538 belongs to the sources which show clear Mg II variability, like NGC 3783 (Reichert et al. 1994), and NGC 4151 (Metzroth et al. 2006), while other objects monitored in Mg II did not show the expected variability, like PG 1247+268 (Trevese et al. 2007). On average, class A sources are less variable in the optical band (e.g. Papadakis et al. 2000; Klimek et al. 2004, Ai et al. 2013) but the example of LBQS 2113+4538 shows that this is not always the case, and the simplicity of the Mg II shape in these sources simplifies the decomposition of the spectrum and the overall monitoring. The Eddington ratio in the source is rather close to 1, but nevertheless we do not see evidence of the Mg II line coming from wind outflow, which would prevent the use of the line for black hole mass and intrinsic luminosity measurement.

Acknowledgements. We are grateful to Dr. Alexey Pamyatnykh for helpful discussion. Part of this work was supported by the Polish grant Nr. 719/N-SALT/2010/0, and the spectroscopic observations reported in this paper were obtained with the Southern African Large Telescope (SALT), proposal SALT/2012-1-POL-008. KH, BC, MK and AS acknowledge the support by the Foundation for Polish Science through the Master/Mistrz program 3/2012. This research has made use of the NASA/IPAC Extragalactic Database (NED) which is operated by the Jet Propulsion Laboratory, California Institute of Technology, under contract with the National Aeronautics and Space Administration. The Fe II theoretical templates described in Bruhweiler & Verner (2008) were downloaded from the web page <http://iacs.cua.edu/personnel/personal-verner-feii.cfm> with the permission of the authors.

References

- Ai, Y.L. et al, 2013, *AJ*, 145, 90
- Bentz, M. C. et al., 2013, *ApJ*, 767, 149
- Boller T., Brandt W. N., Fink H., 1996, *A&A*, 305, 53
- Brandt, W.N., Mathur, S., Elvis, M., 1997, *MNRAS* 285, L25
- Bruhweiler, F., Verner, E., 2008, *ApJ*, 675, 83
- Burgh, E.B. et al. 2003, *SPIE*, 4841, 1463
- Castelli, F., Kurucz, R.L., 2004, *arXiv:astro-ph/0405087*
- Clavel, J., et al., 1991, *ApJ*, 366, 64
- Collin-Souffrin, S., Dyson, J.E., McDowell, J.C., Perry, J.J., 1988, *MNRAS*, 232, 539
- Collin-Souffrin, S., & Dumont, S. 1986, *A&A*, 166, 13
- Collin, S., Kawaguchi, T., Peterson, B.M., Vestergaard, M., 2006, *A&A*, 456, 75
- Contini, M., Rodriguez-Ardila, A., Viegas, S., 2003, *A&A*, 408, 101
- Crawford, S.M. et al., 2010, *PySALT: the SALT Science Pipeline. SPIE Astronomical Instrumentation*, 7737-82.
- Czerny, B., Hryniewicz, K., 2011, *A&A*, 525, L8
- Czerny, B. et al., 2013, *A&A*, 556, A97
- Ferland, G. et al., 2009, *ApJ*, 707, L82
- Forster, K. et al., 2001, *ApJS*, 134, 35
- Gallo, L.C., 2006, *MNRAS*, 368, 479
- Goad, M.R. et al. 1999, *ApJ*, 512, L95
- Grupe, D. 2004, *AJ*, 127, 1799
- Grupe D., Mathur S., 2004, *ApJ*, 606, L41
- Hewett, P.C., Foltz, C.B., Chaffee, F.H. 1995, *AJ*, 109, 1498
- Kaspi, S. et al. 2000, *ApJ*, 533, 631
- Klimek, E. S., Gaskell, C. M., & Hedrick, C. H. 2004, *ApJ*, 609, 69
- Kobulnicky, H.A. et al., 2003, *ApJ*, 599, 1006
- Kollatschny, W., Zetzl, M. 2013, *A&A*, 549, A100
- Kollmeier, J.A. et al., 2006, *ApJ*, 648, 128
- Kong M.-Z., Wu X.-B., Wang R., Han J.-L., 2006, *Chin. J. Astron. Astrophys.*, 6, 396
- Laor, A., Jannuzi, B.T., Green, R.F., Boroson, T.A., 1997, *ApJ*, 489, 656
- Leighly K. M., 1999, *ApJS*, 125, 317
- Marziani, P., Sulentic, J.W., Plauchu-Frayn, I., del Olmo, A., 2013, *arXiv:1301.0520v1*
- Mineshige, S., Kawaguchi, T., Takeuchi, M., & Hayashida, K. 2000, *PASJ*, 52, 499
- McGill, K. L., Woo, J., Treu, T., & Malkan, M. A. 2008, *ApJ*, 673, 703
- McLure, R.J., Dunlop, J.S., 2004, *MNRAS*, 352, 1390
- Morton, D.C., 1991, *ApJS*, 77, 119
- Netzer, H., Laor, A., 1993, *ApJ*, 404, L51
- Osterbrock, D.E., Pogge, R.W., 1985, *ApJ*, 297, 166
- Panessa, F. et al., 2011, *MNRAS*, 432, 1138
- Papadakis, I. E., Brinkmann, W., Negoro, H., Detsis, E., Papamastorakis, I., Gliozzi, M., 2000, *arXiv:astro-ph/0012317*
- Peterson, B.M., 1993, *PASP*, 105, 247
- Peterson, B.M. et al. 2004, *ApJ*, 613, 682
- Piquard, S., et al. 2001, *A&A*, 373, 576
- Pounds, K.A., Done, C., Osborne, J.P., 1995, *MNRAS*, 277, L5
- Reichert, G.A. et al., 1994, *ApJ*, 425, 582
- Schlafly, E.F., Finkbeiner, D.P., 2011, *ApJ*, 737, 103
- Shapovalova, A.I. et al., 2012, *ApJS*, 202, 10
- Shen, Y., Greene, J. E., Strauss, M. A., Richards, G. T., & Schneider, D. P. 2008, *ApJ*, 680, 169
- Smith, M.P. et al., 2006, in *Society of Photo-Optical Instrumentation Engineers (SPIE) Conference Series*, Vol. 6269, *Society of Photo-Optical Instrumentation Engineers (SPIE) Conference Series*
- Sulentic, J.W., Bachev, R., Marziani, P., Negrete, C.A., Doltzin, D., 2007, *ApJ*, 666, 757
- Sulentic, J. W., Marziani, P., Zamanov, R., Bachev, R., Calvani, M., & Dultzin-Hacyan, D. 2002, *ApJ*, 566, L71
- Trakhtenbrot, B., Netzer, H., 2012, *MNRAS*, 427, 3081
- Trevese, D., Paris, D., Stirpe, G. M., Vagnetti, F., & Zitelli, V. 2007, *A&A*, 470, 491
- Tsuzuki, Y., Kawara, K., Yoshi, Y., Oyabu, Sh., Tanabe, T., Matsuoka, Y., 2006, *ApJ*, 650, 5-
- Veron-Cetty, M.P., et al., 2001, *A&A*, 374, 92
- Veron-Cetty M.-P., Veron P., Goncalves A. C., 2001b, *A&A*, 372, 730
- Vestergaard, M., Wilkes, B., 2001, 134, 1
- Vestergaard, M., & Osmer, P. S. 2009, *ApJ*, 699, 800
- Wandel, A., Peterson, B.M., Malkan, M.A., 1999, 526, 419
- Wang J.-M., Netzer H., 2003, *A&A*, 398, 927
- Wang, J.G. et al., 2009, *ApJ*, 707, 1334
- Watson, D. et al. 2011, *ApJ*, 740, L49
- Whalen, D.J., Laurent-Muehleisen, S. A., Moran, E. C., Becker, R. H., 2006, *AJ*, 131, 1948
- Woo, J.-H., 2008, *AJ*, 135, 1849
- Zamfir, S., Sulentic, J.W., Marziani, P., Dulcin, D., 2010, *MNRAS*, 403, 1759-1786